VOL. 18, NO. 18, SEPTEMBER 2023 ISSN 1819-6608
ARPN Journal of Engineering and Applied Sciences

www.arpnjournals.com

PAPR REDUCTION OF FBMC-OQAM SIGNALS USING PHASE SEARCH-PTS AND MODIFIED DISCRETE FOURIER TRANSFORM SPREADING

Karthik Kumar Vaigandla and J. Benita
Electronics and Communication Engineering, Noorul Islam Centre for Higher Education, Kanyakumari, Tamil Nadu, India
E-Mail: vkvaigandla@gmail.com

ABSTRACT

In this research, a novel peak-to-average power ratio (PAPR) reduction technique for filter bank multicarrier (FBMC) modulation systems is presented. With multicarrier systems like FBMC, the strategy focuses on the survival of the fittest principle to suit the value of PAPR. The Filter Bank Multicarrier with Offset Quadrature Amplitude Modulation (FBMC-OQAM) has recently captured the attention of numerous academics due to its minimal adjacent channel leakage ratio (CLR). Unfortunately, the issue of increased PAPR measurement has a negative impact on the effectiveness of the FBMC system's energy measurement. In this study, the Phase search-based Partial Transmit Sequence (PS-PTS) approach and Modified Discrete Fourier Transform Spreading (MDFT) are developed for the PAPR reduction of the FBMC-OQAM signals. The increased PAPR measurement is reduced using the PTS and MDFT with osprey optimization method, which may result in a PAPR reduction of roughly 5.1 dB as comparable to the conventional approach.

Keywords: PAPR, FBMC-OQAM, optimization, PTS, BER.

Manuscript Received 23 August 2023; Revised November 12, 2023; Published November 30, 2023

1. INTRODUCTION

As a substitute to orthogonal frequency division multiplexing (OFDM) in modern systems for wireless communication (such as 5G), filter bank multicarrier (FBMC) is a strong possibility. Like all methods of multicarrier modulation, FBMC has a significant PAPR. In order to reduce PAPR in OFDM-NOMA systems, a novel selective mapping (SLM) technique is suggested. By using the OFDM-NOMA transmitter's structure, the SLM approach delivers similar consequences as the traditional SLM scheme while needing less computing complexity [1]. However, it has been claimed that OFDM-NOMA has experienced nonlinear distortion after passing through nonlinear high-power amplifiers (HPAs) owing to a high PAPR issue. As a consequence, reachable data rates, sum rate capabilities, and users' bit error rate (BER) have all decreased [2]. Humans employ an auxiliary pilot to address the FBMC system's issue with fictitious interference. The PAPR is then decreased using a hybrid technique that combines clipping with filtering and the Vandermonde-like matrix (VLM), which is based on the pilot-assisted FBMC system. The VLM of Chebyshev polynomials precodes the input data to lessen the input signal's autocorrelation. The clipping and filtering module receives the signal next, which further suppresses the PAPR. The multipath channel model was used with the pilot-assisted FBMC [3-4].

Conditions under which the single carrier effect of DFT spreading can be fully utilized by the DFT, hence lowering the PAPR and also recommend an improvement approach that, with no added computational overhead, is applied to the extended DFT for yet more PAPR minimization. In comparison to existing DFT spreading strategies, the GDFT spreading technique and the improved one also exhibit stronger power spectral density (PSD) [5]. An improved structure with the Low Peak-to-average Power Ratio Filter Bank MultiCarrier (LP-FBMC) structure relied on DFT spread; spreading necessitates further transmission Side Information (SI). The complexity is decreased by the local rotation method's reduction in the overall phase rotation angles, and the receiver's accuracy of phase estimate is increased by broadening the phase decision range. Yet, compared to the embedded SI structure, it also decreases the computing cost by around 20% [6].

The FBMC-OQAM currently attracted the interest of numerous academics due to its low adjacent CLR. The issue of high PAPR measurement, however, has a negative impact on the effectiveness of the FBMC system's energy evaluation. This investigates partial transmit sequence (PTS) approaches for PAPR reduction of FBMC-OQAM signals. The system's primary drawback, the bigger PAPR measurement, is addressed in this study by the PTS with a randomized frog leap phase optimization approach [7].

The PAPR and the framework's complexity are reduced effectively by hybrid Selective Mapping (SLM) as well as Partial Transmission Scheme (PTS). In addition, it is clear that the suggested technique is essential to obtaining superior spectral and power attributes in comparison to the current waveforms. For 5G as well as beyond 5G systems, the suggested SLM-PTS dependent NOMA-FBMC structure effectively improves throughput as well as PAPR performance [8]. To lower PAPR without transmitting corner information, dummy sub-carriers based on Particle Swarm Optimization (PSO) and IFFT output (Inverse Fast Fourier Transform) are introduced. To examine PAPR and BER performances, the network structure has been simulated in an AWGN channel configuration [9].

The FBMC-OQAM signal investigates PAPR reduction using a joint PTS (JPTS) and PSO. Utilizing PSO-JPTS's simulations, the FBMC-OQAM technique's PAPR has been demonstrated to be superior to the conventional FBMC-OQAM. The simulation's outcomes also demonstrate how different populations might enhance their complementary cumulative distribution function (CCDF) [10]. To determine the appropriate solution, the PTS requires utilizing the traversal approach, which renders the system more complex. A PTS predicated on discrete PSO with the threshold (PTS-DPSO-TH) is presented and used to the FBMC/OQAM system in order to resolve this shortcoming. Employing DPSO, PTS-DPSO-TH efficiently lowers the FBMC/OQAM system's overly high PAPR while preventing the system's complexities from expanding. To illustrate the performance of PAPR minimization, the threshold is established to limit the amount of iterations and significantly minimize the system's complexity [11].

The contribution of the research as follows:

- This research presents a phase search based PTS (PS-PTS) scheme, subsequently exploiting iterative flipping (IF) as a strategy of optimization.
- In this research, a novel PAPR reduction method for filter bank multicarrier (FBMC) modulation schemes is introduced. With multicarrier systems like FBMC, the strategy builds on the survival of the fittest principle to suit the value of PAPR at an affordable range.
- The proposed PS-PTS and MDFT procedure in association with a osprey optimization algorithm for MIMO relied OQAM-FBMC anticipate a substantial drop in PAPR.
- The increased PAPR measurement is reduced using the PTS and DFT with osprey optimization method, which may result in a PAPR reduction of roughly 5.1 dB as comparable to the conventional approach.

The remainder of the paper is arranged as follows: Section 2 introduces the literature survey. The proposed PAPR mitigation scheme is discussed in Section 3. Section 4 comprises a presentation of the simulation outcomes. The conclusions were explained in Section 5.

2. RELATED WORKS

Samayoa *et al*. [12] introduce the modified active constellation extension (mACE) algorithm. During simulation, the ability of mACE to minimize the PAPR was revealed and its performance is compared to that of the most sophisticated smart gradient-project (SGP) approach. It has been proven that mACE is superior to the SGP technique. These results are attained using less challenging computational techniques. Choi *et al.* [13] upgrade the DFT spreading-based Low PAPR FBMC system to the ICI-free Alamouti-coded FBMC. It initially delivers the adjustments required for combining the two schemes in order to gain the benefits of both. The recommended method still accomplishes the single carrier effect of DFT spreading even with frequency reversal Alamouti code architecture, according to a mathematical investigation.

Yeh *et al*. [14] provide a redesigned method entitled Hadamard Single-Carrier Frequency Division Multiple Access (SCFDMA) for minimizing the PAPR of pulse-shaped signals. Additionally, it examines the Symbol Error Rate (SER) of the proposed Hadamard SCFDMA systems. The results demonstrated that the Hadamard SCFDMA system enhanced SER and minimized complexity in addition to reducing PAPR. In [15] provide techniques for Nonlinear Distortion Reduction Based on Clipping and Compressive Sensing in OFDM/OQAM System. Na et al. [16] proposed a simplified Low PAPR FBMC (LP-FBMC) that does away with the necessity to send SI thus retaining BER performance and add SI information to the phase expression for the full sub-frame without adding any supplementary energy. The receiver could identify the SI by analysing the phase offset of the chosen parameters with a minimal improvement in computation cost.

Nissel *et al*. [17] suggested novel modulation method integrates the features of FBMC-OQAM with single-carrier frequency-division multiple access (SC-FDMA). On top of a conventional FBMC system, it implements a revolutionary precoding technique predicated on a trimmed DFT and one-tap scaling. The proposed approach lacks the need for a cyclic prefix and offers significantly reduced out-of-band emissions while maintaining the same PAPR as SC-FDMA. Hossain *et al*. [18] propose a DFT-Spread OTFS system to successfully decrease the PAPR. The power efficiency in practical wireless communication systems may deteriorate or the BER might be significantly compromised due to the higher peak signal intensity in a high-power amplifier (HPA). Hence, both the HPA's efficiency and the nonlinear distortion it generates could be significantly improved by decreasing the PAPR.

Sarkar *et al.* [19] proposed Twin Symbol Hybrid Optimization (TSHO-PTS), which served as the foundation for the Cyclic Prefix-OFDM Partial Transmit Sequence (PTS) technique (CP-OFDM). The cost of computing PTS may also rise as a result of the thorough search for the ideal phase components and used to address this issue and evaluate the phase factor utilizing the PTS technique as effectively as possible as well as preserve the security of physical layer. Cho et al. [20] published an enhanced general precoding method (GPC) for configurable PAPR reduction in DFT-OFDM. The recommended method has a larger enhancement in PAPR reduction, specifically in decreased modulations, and its effectiveness may be extended to other transmission bandwidths.

Hossain *et al*. [21] recommended a DFT-Spread WR-OFDM (windowing and restructuring OFDM) to establish tolerably permissible upcoming generation mobile as well as wireless systems predicated on the

considerable minimisation including both PAPR and out-of-band (OOB) power spectrum components. AWGN and multipath Rayleigh fading channel system performances are contrasted with those of conventional cyclic prefix(CP) and WR (window and reconstruction) - OFDM systems. A hybrid strategy is suggested by Tang *et al*. [22] is the iterative clipping and filtering (ICF) methodology as well as the enhanced nonlinear companding (ENC) scheme. The analysis's findings demonstrate that while the computational complexity of the suggested method is considerably less than that of ICF, it is marginally greater than that of ENC. Additionally, the simulation results demonstrate that, in comparison to ICF, the suggested technique performs better in terms of PAPR reduction and BER.

Shekh Faraj *et al.* [23] investigate numerous PAPR reduction procedures and contrasted them to identify which methodology is acceptable for a specified technology. The three primary categories of methodologies are distortion, probabilistic, and coding techniques, each of which includes a number of strategies. Increased PAPR yields in the OFDM system's component devices cannot handle the high peaks, leading to distortion and signal loss. Abdulridha *et al.* [24] suggested a hybrid strategy utilizing clipping as well as companding techniques is developed to lower the PAPR of OFDM dependent differential chaos shift keying (OFDM-DCSK), which is the OFDM-primary DCSK's flaw. The complexity of the system is reduced because the receiver does not require an inverse function. The PAPR can be decreased actively through clipping and companding.

Odukwe *et al.* [25] suggested precoding the OFDM signal using the Discrete Cosine Transform (DCT) and adding the Log Companding technique. Based on simulations, three scenarios were taken into consideration to comprehensively investigate the impact of PAPR in the OFDM system. According to the observations, the PAPR of an OFDM signal were decreased by more than half for N = 64 and 256, respectively. Liu *et al*. [26] introduce a generalised continuous piecewise linear companding (CPLC) transform. Due to the considerable function shaping flexibility of these linear segments, it is possible to achieve excellent performance trade-offs among computational sophistication, BER, OOB rejection, as well as PAPR reduction.

Xing *et al*. [27] developed the variation technique dependent nonlinear companding (VANC) strategy to reduce the PAPR in OFDM systems. The required PDF could be identified via addressing a variant optimization challenge modeling that aims to achieve the minimum PDF distortion within restrictions on average signal power as well as probability conservation. Yadav *et al.* [28] suggested a hybrid strategy that incorporates a DFT precoder with a novel error function (NERF) companding. The suggested methodology (DFT precoder with NERF companding) reduces deterioration of bit error rate (BER) effectiveness in combination to PAPR minimization, in contradiction to other recommended alternatives. Niwareeba *et al.* [29] presented a revolutionary hybrid methodology entitled minimal complication hybrid selective mapping (LCHSLM), which incorporates a modified selective mapping (SLM) having companding, with the intention of lowering PAPR in ACO OFDM systems. Computer simulations demonstrate that, particularly compared to the conventional SLM or companding individually, suggested technique substantially minimizes the PAPR. Moreover, LCHSLM provides a considerable complexity minimization without bit error rate (BER) degradation when compared to standard SLM. In [30] provide a modified forest optimization algorithm for FBMC based on SLM, which reduces the PAPR and increases the BER performance. Akurati *et al*. [31] recommended integrating SLM with various types of companding methodologies in order to assist from both approaches. The PAPR is much lower when compared to strategies employing conventional OFDM and OFDM with SLM. Also, it increases spectrum efficiency and decreases system complexity.

Ramadevi*et al.* [32] provide a hybrid Maximal-Minimum approach with deconstructed selective mapping for 5 G Universal Filtered Multi-carrier (UFMC) systems to reduce PAPR constraints. In each branch, real and fake variables are blended with a number of phase vectors. The PAPR settings are customized for each user, and the FIR response is reproduced before transmission. In terms of BER minimization, it is superior to decomposed-UFMC-SLM and selective mapping (SLM).DNN and RNN, a revolutionary, optimal hybrid deep learning technique, was created by Raveen et al. [33] by combining deep neural networks (DNN) and recurrent neural networks (RNN). Yet, there are issues with OFDM as well. One of them, and the primary problem with OFDM, is the high PAPR of the transmitted signal. Because in deep learning, PAPR performance has significantly improved in recent years. Another significant flaw in the OFDM system is the enormous volume of training data and hefty computing expenses.

3. PROPOSED PAPR REDUCTION FOR FBMC/OQAM

3.1 FBMC/OQAM System

Figure-1 depicts the structure of the FBMC/OQAM transmitter, which sends M data blocks in a row via N parallel sub-channels. The definition of the m^{th} input data block vector seems to be:

$$X_m = \left[X_1^m, X_2^m, ..., X_N^m \right]^T \quad (1)$$

where $[.]^T$ and X_k^mstand for the transposition and the k^{th} subcarrier's m^{th} complex input symbol, correspondingly. As an instance, the complex symbol X_k^m would seem to be:

$$X_k^m = a_k^m + jb_k^m \quad (2)$$

where, $a_k^m = H\{X_k^m\}$ and $b_k^m = ð\{X_k^m\}$.$H\ \{\cdot\}$ and $ð\{\cdot\}$ represents the real as well as imaginary parts of a symbol, accordingly. The subcarrier as well as data block indexes typically designated by k and m, respectively, with ranges being $1 \le k \le N$ and $1 \le m \le M$. The numbers M and N describe the data block numbers as well as subcarrier, respectively.

As a result, the data matrix X describing the input data block with M complex values would be interpreted as:

$$X = \left[X^1, X^2, ...X^m, ..., X^M \right] \quad (3)$$

Each X_k^mcomponent throughout the OQAM pre-processing undergoes a staggering procedure in which the real as well as imaginary parts being interconnected by *T/2* to create OQAM symbols, whereby T specifies the time period of a block. Consequently, the N subcarriers of the modulated symbols, being added together to create the m^{th} transmitted FBMC/OQAM data block [34]. The time-domain formulation of the m^{th} FBMC-OQAM data block signal has been provided by equation (4).

$$S^m(t) = \sum_{k=1}^{N} \left[\left\{ \begin{matrix} a_k^m h(t-(m-1)T) + \\ jb_k^m h(t-(m-1)\frac{T}{2}) \end{matrix} \right\} e^{j(k-1)\phi_t} \right]; \quad (4)$$
$$for \quad (m-1)T \le t \le \left(m+k-\frac{1}{2} \right) T$$

where, $\phi_t = \left(\frac{2\pi t}{T} + \frac{\pi}{2}\right)$and h(t) represent for the prototype filter's phase component and impulse response, correspondingly. The M FBMC data blocks subsequently combined together as illustrated in equation (5) to produce the resulting FBMC/OQAM signal S(t):

$$S(t) = \sum_{m=1}^{M} \sum_{k=1}^{N} \left[\left\{ \begin{matrix} a_k^m h\left(t-(m-1)T\right) + \\ jb_k^m h\left(t-(m-1)T-\frac{T}{2}\right) \end{matrix} \right\} e^{j(k-1)\phi_t} \right]; \quad (5)$$
$$for \quad 0T \le t \le \left(m+k-\frac{1}{2} \right) T$$

As a consequence, the filter is employed as the default filter in this research exploration. Also, it is clear that neighbouring data blocks overlap assuming the time period of the prototype filter as well as the stagger among each FBMC symbol's real as well as imaginary components.

3.2 PAPR of FBMC/OQAM Signals

For discrete-time domain signals, the PAPR reduction methodology is employed. Hence, via sampling, the FBMC/OQAM signal was altered into the discrete-time domain, where TF characterizes the sample period, F = LN and L is the oversampling factor. Equation (6) represents the interpretation of the modulated FBMC/OQAM signal during sample n.

$$S[n] = \sum_{m=1}^{M} \sum_{k=1}^{N} \left[\left\{ \begin{matrix} a_k^m h\left(n-(m-1)F\right) + \\ jb_k^m h\left(n-(m-1)F-\frac{F}{2}\right) \end{matrix} \right\} e^{j(k-1)\phi_t} \right]; \quad (6)$$
$$for \quad 1 \le n \le (m+k)F$$

where h[n] symbolizes for a discrete sequence filter which is expressed as a discrete time filter as well as were constructed employing a frequency sampling technique. Equation (7) describes the PHYDYAS filter's impulse response interpretation.

$$h(t) = H_0 + 2\sum_{k=1}^{K} (-1)^k H_k \cos\left(\frac{2\Pi kt}{KT} \right); t \in \left[0, KT\right] \quad (7)$$

The discrete-time parameterization of the PHYDYAS appears as follows when the Nyquist sampling rate being introduced to the function h(t):

$$h(n) = 1 + 2\sum_{k=1}^{K} (-1)^k H_k \cos\left(\frac{2\Pi kn}{KN} \right); n = 1, .., L_p \quad (8)$$

where H_k specifies the filter coefficients defined via:

$$H_0 = 1; H_1 = 0.971; H_2 = 0.707; H_3 = 0.235 \quad (9)$$

By separating S[n], the output sequence into (M + K) successive signal segments, each possessing length corresponding to F samples, it is possible to estimate the PAPR of the signal having M data blocks. Thus, equation (10) could be employed to predict the PAPR in the j^{th} segment

$$PAPR_j = \frac{\left|S\left[n\right]\right|^2}{E\left[\left|S\left[n\right]\right|^2\right]}; 1 \le j \le M+K \quad (10)$$

where $max|S[n]|^2$represents the peak power (P_j) in the jth segment and $E[\cdot]$ becomes the expectation operator. CCDF typically employed to estimate how frequently the PAPR of the signal surpasses a specified threshold ($PAPR_{TH}$), as specified:

$$CCDF_{(PAPR>PAPR)_{TH}} = \frac{\sum_{i=1}^{I} \sum_{j=1}^{M+K} \eta_{j,i}}{(M+K)I} \quad (11)$$

where I remains the amount of simulation trials, and

$$\eta_{j,i} = \begin{cases} 1; & PAPR_j \ \& \ i^{th} best > PAPR_{TH} \\ 0; & elsewhere \end{cases} \quad (12)$$

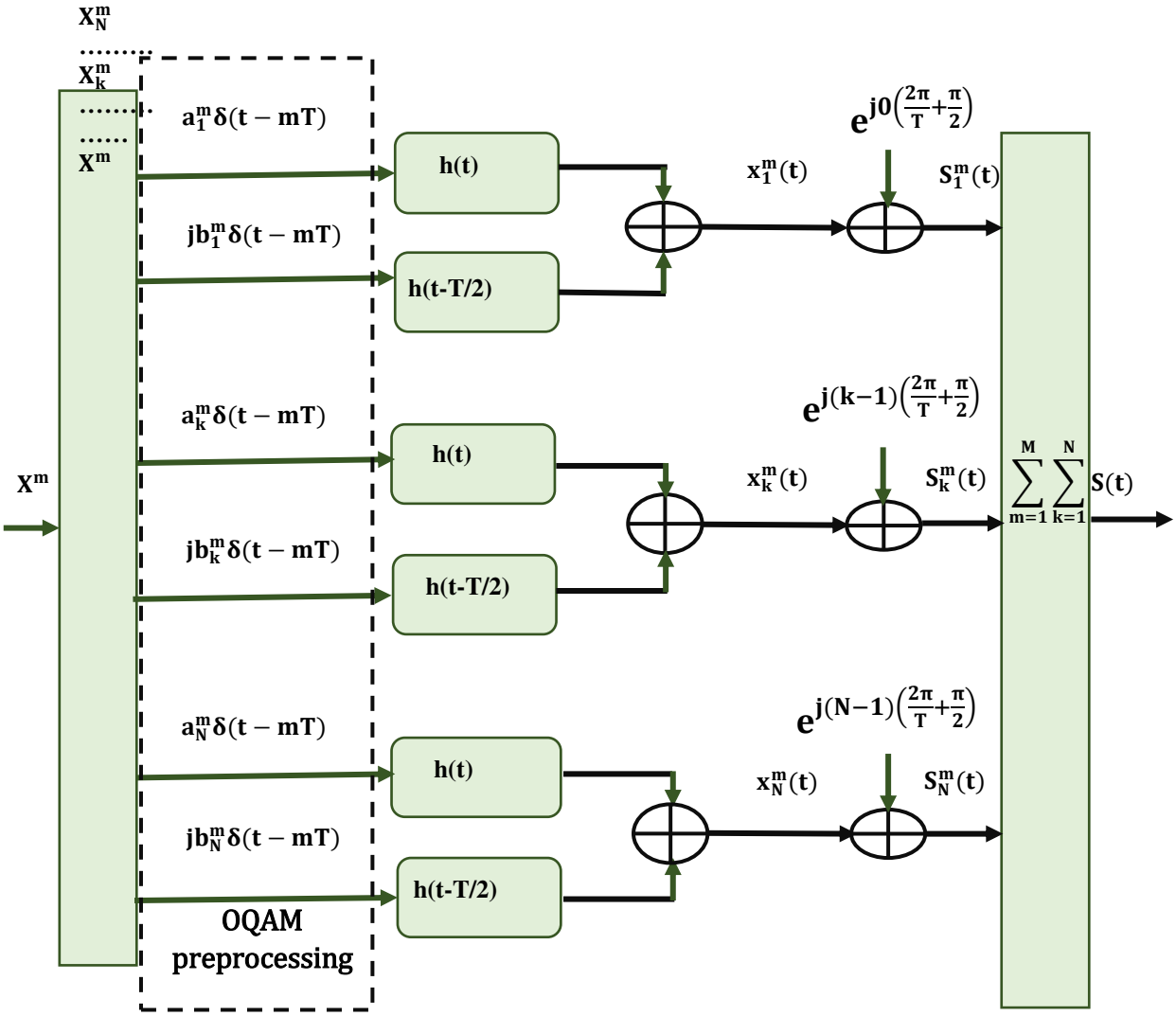

Figure-1. Proposed FBMC/OQAM transmitter.

3.3 Proposed Enhanced-PTS PAPR Reduction Scheme

The functioning of the suggested PAPR reduction strategy is illustrated in this subsection. The initial two operational phases of the suggested method concentrate on generating the PS-PTS signal sub-block segments of the signal. The initial FBMC/OQAM data block subsequently goes through a partitioning mechanism identical to that employed in conventional PTS to generate signals in V sub-blocks, typically with a length of $(K + 1/2)F$, termed as a block of sub-blocks that is thereafter buffered.

The second FBMC data block was therefore subjected to the partitioning procedure. The overlapped component of the previous block is thereafter appended to the resultant block of sub-blocks, and finally the non-overlapping section of the previous block gets buffered after that. The third data block performs equivalent procedures to those in the second block, and the result block of sub-blocks is then buffered after the non-overlapping part of the first block.

For the fourth FBMC data block, the procedures are repeated, and so on unless all the data blocks have been processed in this manner. A block of V FBMC/OQAM sub-blocks with the length $(K + M - 1/2)F$ samples is gradually accomplished. The block of sub-blocks is divided into $(M + K)$ signal segments with a length of F in the second stage. In order to maximize the reduction of signal peaks and prevent spectral re-growth, the overlapping characteristic of the FBMC data blocks is brought into consideration in the composition of the block of sub-blocks.

Iterative flipping is used as a phase factor's search approach to find the candidate signals within every segment. The enhanced PTS with iterative flipping (PS-PTS), which is the suggested PAPR reduction methodology, seems to be the consequence of employing this method of optimizing the signal sub-block segments.

3.4 Modified DFT Spreading with Pulse Shaping Technique

Incorporating the principle of pulse shaping could strengthen the DFT spreading method's capacity to reduce PAPR. Finding an effective transmitter and corresponding receiver wave with the lowest peak power ratio for the channel circumstances provides the theory behind pulse shaping. Because it can lower the ISI, the raised cosine filter is utilized for pulse shaping. Pulse shaping is a linear filtering technique employed to lower the energy of out-of-band signals. The modulated subcarrier and filter impulse response might be utilized in a transmitter to execute the pulse shaping function.

The preceding equation provides the baseband pulse amplitude modulation (PAM) response.

$$S_{PAM}(t) = \sum_{n=-\infty}^{\infty} C_n h(t - nT) \tag{13}$$

Thus, C_n indicates the transmitted symbol, $S_{PAM}(t)$denotes the outcome of PAM, and h(t) symbolizes the impulse response of the pulse shaping filter. It must be emphasized that the impulse response of the filter should still be chosen so that it possesses a minimal bandwidth utilization and zero ISI. The filter's impulse response is mathematically stated as follows for transmission with minimal distortion:

$$h(nT) = \begin{cases} 1; & n = 0 \\ 0; & n = \pm 1, \pm 2, \ldots \end{cases} \tag{14}$$

Here is a description of the pulse shaping filter:

$$S(t) = \sin c\left(\frac{t}{T}\right) \frac{\cos\left(\frac{\Pi \beta t}{T}\right)}{1 - \frac{4\beta^2 t^2}{T^2}} \tag{15}$$

where β seems to be the roll off factor as well as T becomes the symbol period. To estimate the excessive bandwidth of the Nyquist ISI free pulse, here uses the roll-off factor. By adjusting the roll factor following IFFT, the PAPR effectiveness of DFT spreading could be significantly enhanced.

3.5 Proposed PS-PTS and Modified DFT

The PS-PTS methodology employs iterative flipping to progressively optimize the sub-block segments.

Step i: By dividing and sequentially buffering the M FBMC discrete-time data blocks, a block of V FBMC/OQAM subblock signals were constructed. In order to accomplish this, a block of V overlapping OQAM-FBMC sub-blocks having length ($K + M - 1/2$) *F*is generated and $\hat{S}^v[n]$ denotes the v^{th} sub-block's sequence in that block.

$$\hat{S}^v[n] = \sum_{m=1}^{M} \hat{S}^{m,v}[n] \tag{16}$$

Step ii: Create ($M + K$) segments of V successive FBMC/OQAM sub-blocks, typically with a length of F, from the block achieved in step i. The sequence of the v^{th} subblock in the v^{th} segment is demonstrated here by the notation $\hat{S}_q^v[n]$. The segmented block of FBMC/OQAM sub-blocks is depicted in Figure-2.

Step iii: Initialize the phase factor vector (i.e., set $\varphi^{q,v} = 1, v = 1,2,\ldots,V$) for q = 1. After that, determine the $PAPR_q$ of S_q[n], the concatenated sequence in the q^{th} segment, and designate it the label $PAPR_{min}$. As a consequence, the accompanying is a possible signal for the q^{th} segment:

$$\hat{S}^q[n] = \sum_{v=1}^{V} \varphi^{q,v} \hat{S}^v[n]; (q-1)F + 1 \le n \le qF \tag{17}$$

Where $\varphi^{q,v} \in \left\{ e^{\frac{j2\Pi i}{W}}; i = 0,1,..,W-1 \right\}$.

Step iv: Recompute the new $PAPR_q$ of S_q[n] by inverting the first phase factor (v = 1) $\varphi^{q,v} = -1$. If the newer $PAPR_q$ is higher than the $PAPR_{min}$, update $\varphi^{q,1}$ to the old value; alternatively, leave $\varphi^{q,v} = -1$ and update $PAPR_q = PAPR_{min}$.

Step v: For v = 2, execute step iv, and so forth, unless all alternatives for modifying the phase factor's signs have been evaluated (i.e., $v = V$). Equation (18) offers the optimum phase factor vector over the q^{th} segment as an outcome.

$$\varphi_{opt}^{q} = \left\{ \left| \hat{S}^q[n] \right|^2 \right\} \tag{18}$$

Where $\varphi_{opt}^{q} = [\varphi_{opt}^{q,1}, \varphi_{opt}^{q,2}, \ldots, \varphi_{opt}^{q,V}]$.

Step vi: Determine the best candidate sequence for the q[th] segment using the information in (19).

$$\hat{S}_{opt}^{q}[n] = \sum_{v=1}^{V} \varphi_{opt}^{q,v} \hat{S}_q^v[n], \tag{19}$$

Step vii: Repeating steps (iii) through (vi), then assign q = 2, and so on, processing each segment in turn. In conclusion, a series of ($M + K$) consecutive signal segments with the lowest PAPR is the ideal FBMC/OQAM output signal. The ideal discrete-time FBMC/OQAM sequence is symbolized by the symbol "$\hat{S}^{opt}[n]$ ".

In this approach, the PS-PTS is followed by the MDCT. The DCT transform being employed to lower the input sequence's autocorrelation, thereby decreases the

PAPR difficulty and eliminates the requirement to provide side information (SI) to the receiver.

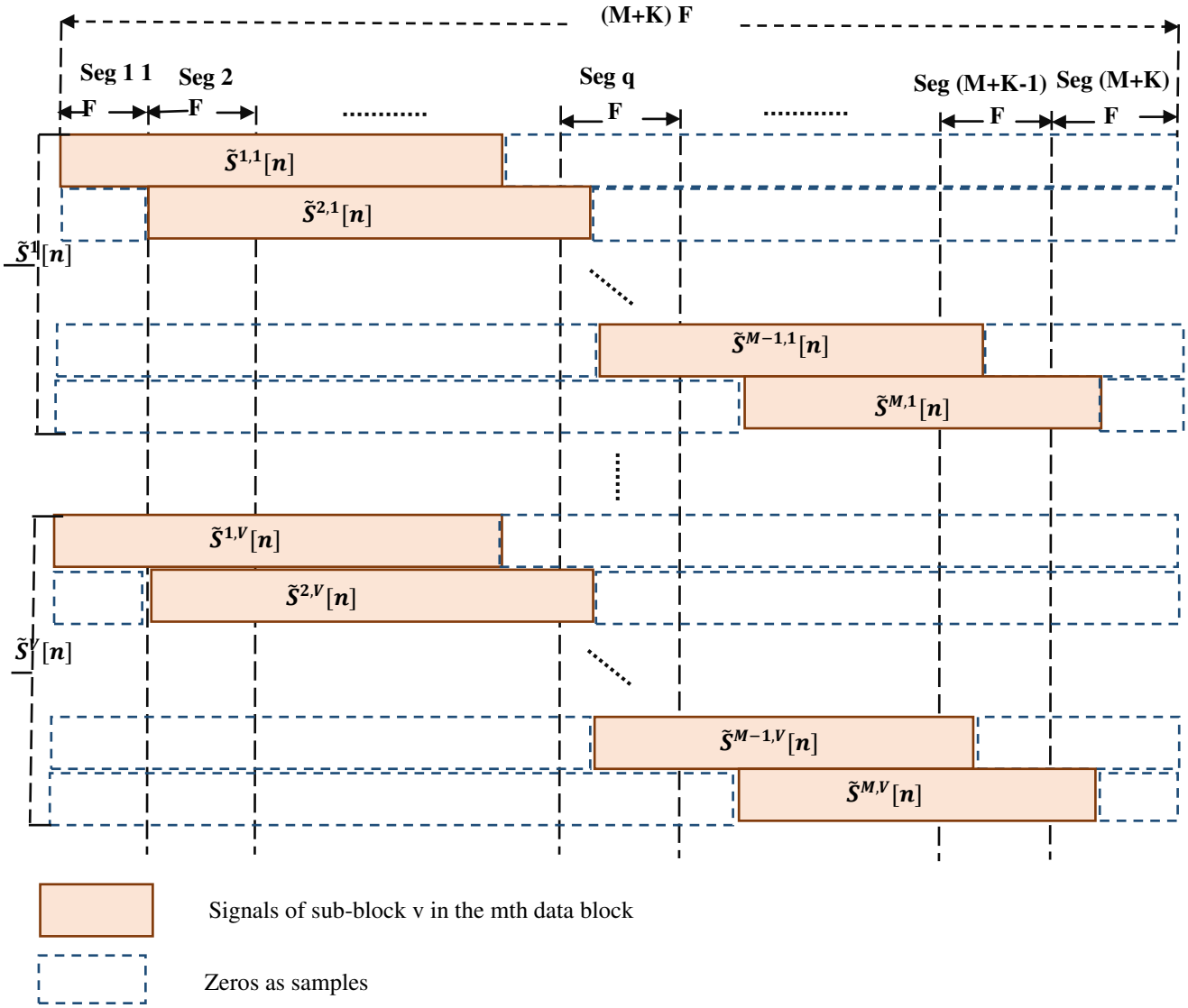

Figure-2. Segmented sub-blocks in the PS-PTS scheme.

3.6 Osprey Optimization Algorithm (OOA)

A novel optimization method might be constructed employing the osprey's hunting tactics and natural abilities to transfer prey to an appropriate location for consumption. Thus, in the formulation of the suggested OOA technique, which is described in the subsequent parts, mathematical modeling of the intelligent osprey activities would be used.

3.5.1 Initialization

Each osprey chooses values related to the issue parameters predicated on its location in the search space as a participant of the OOA population. As a result, each osprey represents a potential solution to the issue, expressed numerically by a vector. When OOA is first implemented, the location of ospreys in the search area is configured arbitrarily utilizing (20).

$$x_{i,j} = lb_j + r_{i,j}(ub_j - lb_j); for \begin{matrix} i = 1,2,..,N \\ j = 1,2,..,m \end{matrix} \quad (20)$$

3.5.2 Phase 1: locating certain locations and fishing (exploration): Due to their keen eyesight, ospreys are powerful hunters who can locate fish underwater. They locate the fish, attack it, and chase the fish by diving under the surface. Depending on a modeling of this typical osprey activity, the first stage of population updating in OOA is modelled. The placements of other ospreys present in the search space that posesses a higher objective function value are regarded as undersea fishes for every osprey in OOA design. An osprey's set of fish is determined using (21).

$$FP_i = \{X_k | k\epsilon\{1,2,\ldots,N\} \wedge F_k < F_i\} \cup \{X_{best}\} \quad (21)$$

Perhaps the optimal candidate solution becomes X_{best} and FP_i represents the collection of fish locations for the i^{th} osprey (the best osprey). One of these fish is randomly located by the osprey, which thereafter strikes it. A new position for the matching osprey was determined using the simulation of the bird's approach toward the fish (22) & (23). If this latest position enhances the desired function's value, the osprey would acquire the position of its old position (24).

$$x_{i,j}^{p1} = x_{i,j} + r_{i,j} \cdot \left(SF_{i,j} - I_{i,j} \cdot x_{i,j}\right) \tag{22}$$

$$x_{i,j}^{p1} = \begin{cases} x_{i,j}^{p1};\ lb_j \le x_{i,j}^{p1} \le ub_j \\ lb_j;\ x_{i,j}^{p1} \le lb_j \\ ub_j;\ x_{i,j}^{p1} \le ub_j \end{cases} \tag{23}$$

$$X_i = \begin{cases} X_i^{P1}; F_i^{P1} < F_i \\ X_i;\ else \end{cases} \tag{24}$$

where SF_i represents the chosen fish for the i^{th} osprey, $SF_{i,j}$ becomes osprey's j^{th} dimension, $r_{i,j}$ were randomized integers in the interval [0, 1], and $I_{i,j}$were randomly initialized from the set {1,2}. X_i^{P1}denotes the new position of the i[th] osprey depending on the initial stage of OOA.

3.5.3 Phase 2: Transferring the fish towards the appropriate location (exploitation):

The osprey brings the fish it has just caught to a suitable (and safe) location so that it can be eaten. Predicated on a simulation of this osprey's real behavior, the second stage of upgrading the population in OOA was modelled. The osprey's positioning in the search space being produced by minor modifications caused by the modeling of transporting the fish toward the proper location, which increases the OOA's exploitation power.

A unique randomized position was computed with each individual in the region as a "fine position for consuming fish" using the OOA design in order to imitate this behavior of ospreys in nature (25) &(26). Therefore, if the goal function's value is higher in this new position, it substitutes the corresponding osprey's former position in accordance with (27).

$$x_{i,j}^{p1} = x_{i,j} + \frac{lb_j + r_{i,j}(ub_j - lb_j)}{t} \; for \begin{cases} i = 1, 2, ., N \\ j = 1, 2, ., m \\ t = 1, 2, ., T \end{cases} \tag{25}$$

$$x_{i,j}^{p2} = \begin{cases} x_{i,j}^{p2};\ lb_j \le x_{i,j}^{p2} \le ub_j \\ lb_j;\ x_{i,j}^{p2} \le lb_j \\ ub_j;\ x_{i,j}^{p2} \le ub_j \end{cases} \tag{26}$$

$$X_i = \begin{cases} X_i^{P2}; F_i^{P2} < F_i \\ X_i;\ else \end{cases} \tag{27}$$

where $r_{i,j}$ seem to be randomized integers in the range [0, 1], X_i^{P2}indicates the new location of the i[th] osprey predicated on the following stage of OOA,$x_{i,j}^{p2}$provides its j^{th} dimension, F_i^{P2} seems to be its objective function value, t indicates the algorithm's iteration timer, and T symbolizes the overall number of repetitions.

In order to receive the lowest PAPR, the PAPR optimization issue is therefore addressed by locating the ideal phase factor, or $\varphi^{q,v}$. The fitness function (FP_i) is constrained by selecting the highest attainable value.

The loop is broken if FP_i falls below the greatest allowable limit or if there are more iterations than the highest allowable number. In order to get the lowest PAPR, the PAPR optimization problem is therefore solved by locating the ideal phase factor, or $\varphi^{q,v}$.

4. RESULTS AND DISCUSSIONS

In this section, in-depth simulations were undertaken to assess how effectively the suggested PS-PTS technique reduced PAPR when contrasted to the PSO-JPTS and TSHO-PTS schemes. The default filter is the PHYDYAS filter with length $Lp = KLN$. The allowable phase factors is set to W = 2, which represents that all phase rotation factors were selected from the range of {+1, −1}. Furthermore, sub-block partitioning is done using adjacent partitions. CCDF is used to quantify the PAPR. Table-1 contains all of the values for the simulation variables.

Figure-3 shows the PSO-JPTS scheme's performance when OQAM modulation order, N = 128 subcarriers, and various numbers of sub-blocks are employed. In this instance, the PSO-JPTS technique were applied immediately to the FBMC/OQAM, and the signal's PAPRs at CCDF of 10^{-3} were 11.1dB, 8.2dB, 7.1dB and 4.7dB for the FBMC/OQAM signal for the PSO-JPTS various sub-blocks. It is clear that when the number of sub-blocks rises, the value of PAPR falls. Nevertheless, even employing a significant amount of sub-blocks (V = 16), the PAPR of 4.7dB were accomplished, and as a result, the PSO-JPTS is unable to accommodate the high PAPR in the FBMC/OQAM signal adequately. This demonstrates that there is no corresponding PAPR decrease when PTS-based methods are being used directly in the FBMC/OQAM signal. Also, the PSO-exponential

JPTS's computing cost is a result of its thorough examination of phase rotation parameters.

Table-1. Simulation parameters.

Parameters	Value
Simulation Tool	MATLAB
Technique	FBMC/OQAM
Oversampling factor (L)	8
Sub-blocks	2, 4, 8, 16
Number of subcarriers (N)	128
Overlapping factor	4
Modulation	OQAM
Channel	AWGN
FFT Length	1024
Data block	10^{-3}
CP of length	64
phase factors W = 2	+1, -1

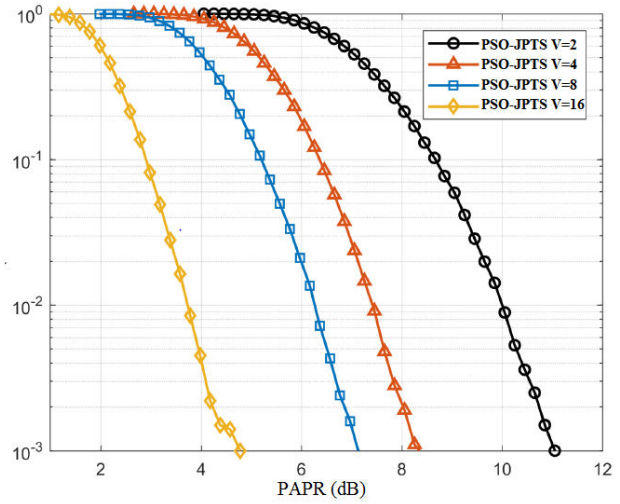

Figure-3. Performance for FBMC/OQAM signal using CCDF versus PAPR with PSO-JPTS scheme.

The effectiveness of the TSHO-PTS technique when applied directly to the FBMC/OQAM signal was assessed in Figure-4. In the simulation, a OQAM modulation scheme with 128 subcarriers including various sub-block numbers between 2 and 16 was employed, which is equivalent towards the C-PTS. With a gain of 1.7 dB over the signal, the TSHO-PTS scheme's PAPR reduction performance for V = 16 is comparable to that of the PSO-JPTS approach. The I-PTS technique achieves a PAPR reduction of 1.7 dB with CCDF =10^{-3} when 16 sub-blocks are used. Because of this, although having a lower computational complexity than PSO-JPTS, the simple application of TSHO-PTS to the FBMC signal would not result in a superior enhancement in PAPR suppression.

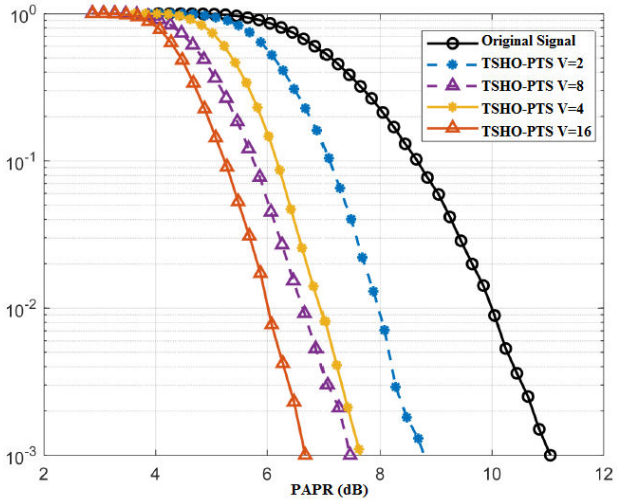

Figure-4. Performance for FBMC/OQAM signal using CCDF versus PAPR with TSHO-PTS scheme.

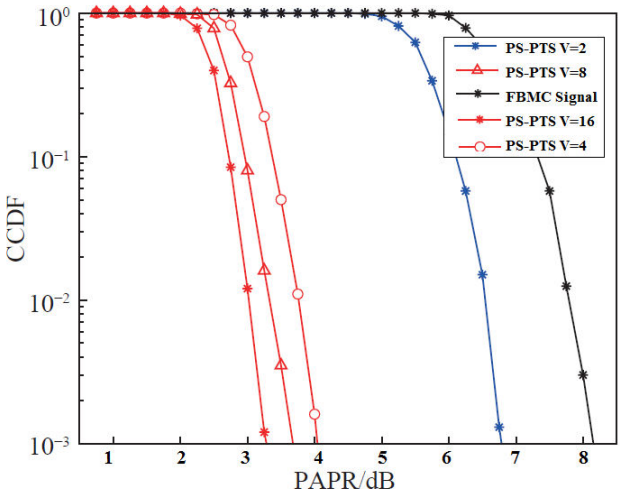

Figure-5. Performance for FBMC/OQAM signal using CCDF versus PAPR with PS-PTS scheme.

The results shown in Figure-5 depicts the PAPR performance of the PS-PTS scheme under OQAM modulation when N = 128, W = 2 and various sub-blocks. The PAPR for the initial signal, which is roughly 8.1 dB, is illustrated by the FBMC/OQAM graph. The PAPR reduction gain attained by the PS-PTS with respect to the original signal when subblocks are 2, 4, 8 and 16, correspondingly, is about 1.5 dB, 4.1dB, 4.6dB and 5.1dB, respectively, according to the CCDF at 10^{-3}. As a result, the PS-PTS algorithm possesses the best PAPR reduction performance.

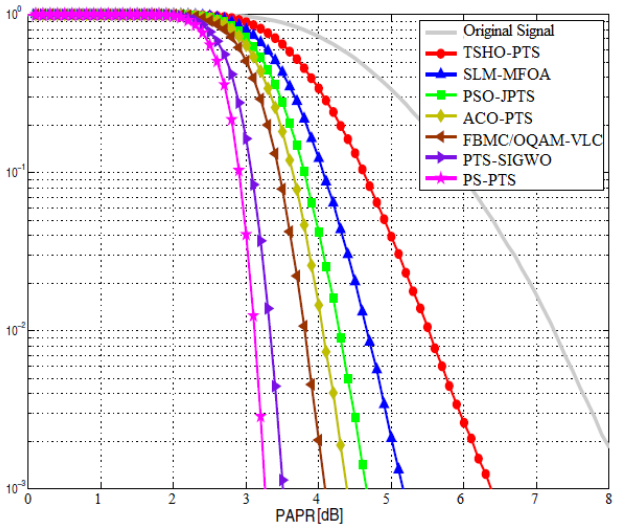

Figure-6. Performance for FBMC/OQAM signal using CCDF versus PAPR, PSO-PTS and various methods.

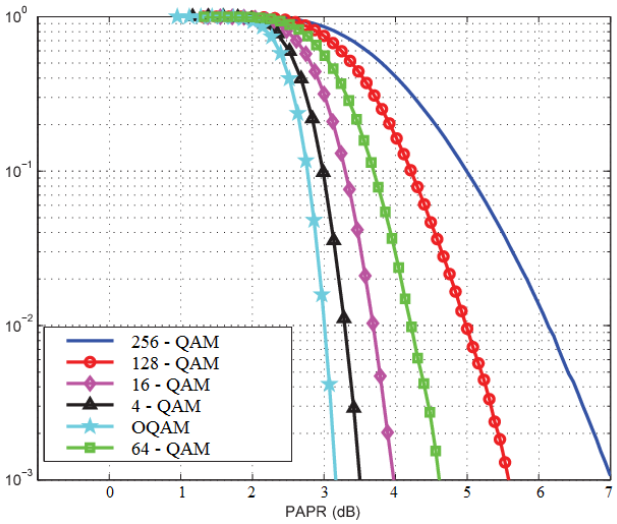

Figure-7. PAPR for various QAM values.

The performance of the suggested algorithm compared to the original FBMC signal and other PAPR minimization methodologies, such as the PSO-JPTS, SLM-MFOA, ACO-PTS, PTS-SIGWO, TSHO-PTS and FBMC\OQAM-VLC approaches, is summarized in Figure-6. While simulating, OQAM modulation was used, and the variables N, V, and W have been assigned to 128, 16, and 2, correspondingly. According to the simulation outcomes, the FBMC signal, TSHO -PTS, SLM-MFOA, PSO-JPTS, ACO-PTS, FBMC/OQAM-VLC and PTS-SIGWO approaches, respectively, possess PAPRs of 8.2 dB, 6.4 dB, 5.2dB, 4.7dB, 4.5dB, 4.2dB, 3.3dB and 3.1dB. The PAPR of the initial signal dropped to 5.1dB after utilizing the PS-PTS method. This shows that the PS-PTS scheme obtains PAPR reduction of approximately 1.8dB, 3dB, 3.5dB, 3.7dB, 4dB, 4.9dB and 5.1dB over the TSHO-PTS, SLM-MFOA, PSO-JPTS, ACO-PTS, FBMC/OQAM-VLC and PTS-SIGWO methods. This is an important accomplishment, especially in context of the fact that, in contrast to the C-PTS algorithm, the PS-PTS algorithm uses a suboptimal search technique. Moreover, due to an enhancement in computational complexity, the PAPR effectiveness of the C-PTS only marginally improves in comparison to the TSHO-PTS. The proposed method gives an acceptable PAPR reduction gain, is fewer difficult, and operates noticeably better than the other techniques.

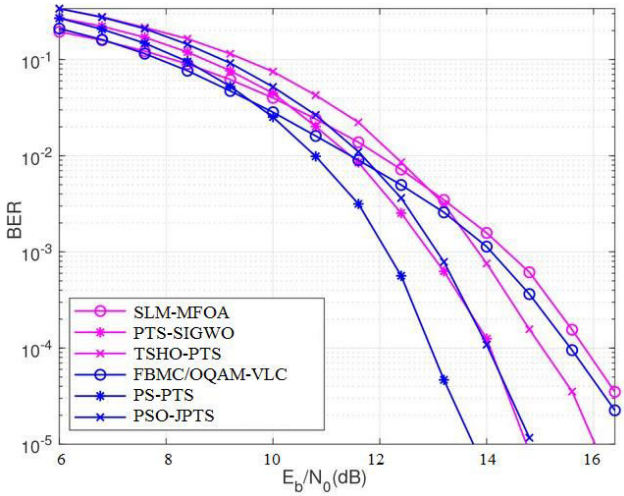

Figure-8. BER performance.

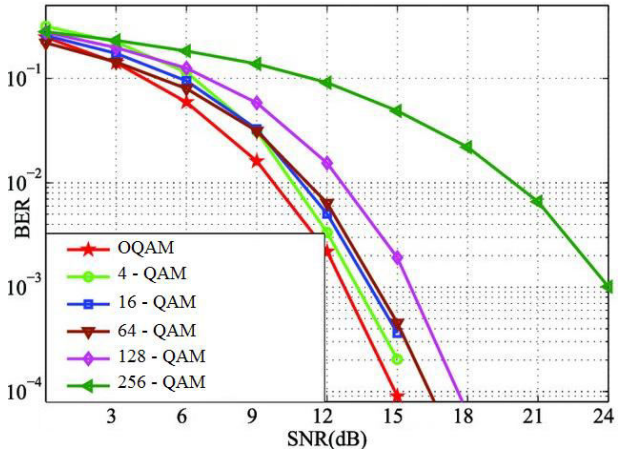

Figure-9. BER performance for various QAM values.

The BER performance for the proposed PS-PTS system is shown in Figure-8. When compared to the other methods, the suggested PAPR reduction technique offers higher BER performance. At a CCDF of 10^{-3}, the SNR values are 15dB, 14.2dB, 13.7dB, 13.1dB, 12.5dB and 12.1dB for the methods of SLM-MFOA, FBMC/OQAM-VLC, TSHO-PTS, PSO-JPTS, PTS-SIGWO and PS-PTS, respectively. The proposed method provides better BER performance, in comparison to other techniques.

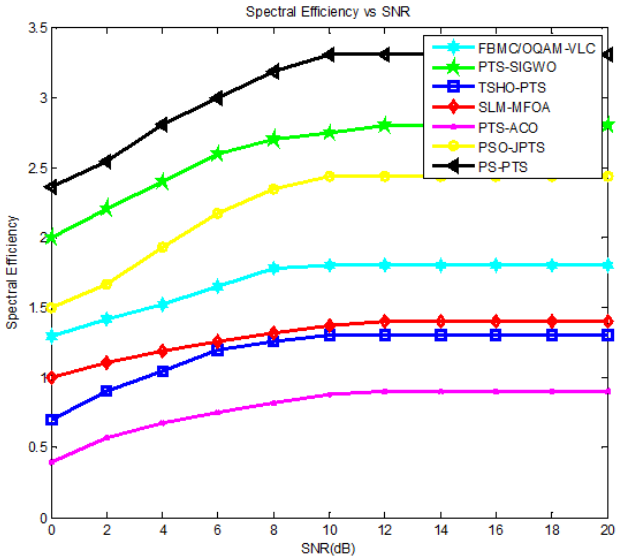

Figure-10. Spectral efficiency comparison.

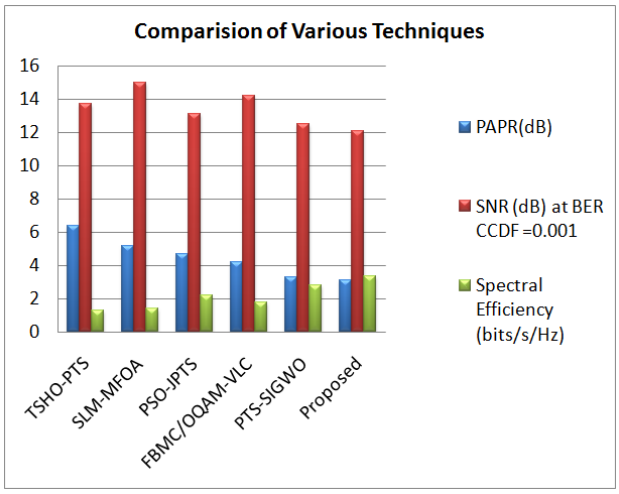

Figure-11. Comparisons using various schemes.

The spectral efficiency (SE) for the proposed PTS and other techniques is shown in Figure-10. The performance of FBMC/OQAM system can be evaluated by spectral efficiency (SE). When compared to the other methods, the suggested PAPR reduction technique offers higher spectral efficiency. For SNR of 20 dB, the SE of proposed method is 3.35. The SE of PTS-SIGWO, PTS-JPTS, FBMC/OQAM-VLC, SLM-MFOA, TSHO-PTS and PTS-ACO is 2.8, 2.48, 1.8, 1.4, 1.3 and 0.85, respectively. The proposed method provides better spectrum efficiency as compared to the FBMC/OQAM-VLC, PSO-JPTS, SLM-MFOA, PTS-ACO, PTS-SIGWO and other methods.

5. CONCLUSIONS

In order to lower the excessive PAPR in the FBMC/OQAM system, a technique for minimizing PAPR was presented out in this research. The FBMC/OQAM data blocks were divided into sub-blocks, and the overlaps among them were brought into account for buffering. Then, employing a suboptimal combinatorial search strategy, the aggregate partitioned data blocks became separated into a number of segments of sub-blocks. As a consequence, the suggested PS-PTS technique is a very practical PAPR lowering technique that might be used well for the FBMC/OQAM signals. In order to optimize the phase rotation parameters for PAPR minimization in FBMC/OQAM systems, this research investigated. The PTS and DFT with Osprey optimization method is used to lower the increased PAPR measurement, which might lead to a PAPR reduction of about 3.1 dB in comparison to the traditional methodology.

Conflicts of Interest

The authors declare that there is no conflict of interest.

Funding Statement

No funding.

ACKNOWLEDGMENT

The authors are grateful to the management of Noorul Islam Centre for Higher Education (Deemed-to-be-University), Thuckalay, Kumaracoil, Kanyakumari, Tamil Nadu-629180, for their support during the research work.

REFERENCES

[1] Karthik Kumar Vaigandla, Dr. J. Benita. 2022. Study and Analysis of Various PAPR Minimization Methods. International Journal of Early Childhood Special Education (INT-JECS). 14(03): 1731-1740.

[2] Mounir Mohamed, Mohamed Ibrahim Youssef and Ashraf Mohamed Aboshosha. 2023. Low-complexity selective mapping technique for PAPR reduction in downlink power domain OFDM-NOMA. EURASIP Journal on Advances in Signal Processing. 2023(1): 10.

[3] Mounir Mohamed, Mohamed Ibrahim Youssef and Ashraf Mohamed Aboshosha. 2023. Low-complexity selective mapping technique for PAPR reduction in downlink power domain OFDM-NOMA. EURASIP Journal on Advances in Signal Processing. 2023(1): 10.

[4] Liu Song, Yue Li and Jianqiang Wang. 2019. Hybrid peak-to-average-power-ratio reduction method based on filter bank multicarrier in wireless sensor networks. Sensors and materials. 31(12): 3999-4011.

[5] Aboul-Dahab, Mohamed A., Mohamed M. Fouad, and Radwa A. Roshdy. 2019. Generalized discrete

Fourier transform for FBMC peak to average power ratio reduction. IEEE access. 7: 81730-81740.

[6] ZHAO Hui, Wei WANG, Jinrong MO and Tianqi ZHANG. 2022. Structure Optimization of Low Peak-to-average Power Ratio Filter Bank MultiCarrier Based on Constellation Symbol Sequence Local Phase Rotation. 44(2): 668-676.

[7] Kumar Ch Thejesh, Amit Bindaj Karpurapu, and Mayank Mathur. 2022. Analysis of peak-to-average power ratio in filter bank multicarrier with offset quadrature amplitude modulation systems using partial transmit sequence with shuffled frog leap optimization technique. ACTA IMEKO. 11(1): 5.

[8] Sharma M. K. and A. Kumar. 2022. Analysis of Peak to Average Power in the 5G NOMA-FBMC Waveform. Indian Journal of Science and Technology 15, no. 41 (2022): 2182-2187.

[9] Abed Ahmed K., Riyadh Mansoor and Ali K. Abed. 2022. Particle Swarm Optimization-based dummy sub-carriers insertion for peak to average power ratio reduction in OFDM systems. ICT Express. 8(1): 135-141.

[10] Rajendra Prasad, D., S. Tamil and Bharti Chourasia. 2022. PAPR Reduction for FBMC-OQAM Signals Using PSO-Based JPTS Scheme. In Innovations in Electronics and Communication Engineering: Proceedings of the 9th ICIECE 2021, pp. 29-38. Singapore: Springer Singapore.

[11] Li Lei, Lunsheng Xue, Xihong Chen, and Dizhe Yuan. 2022. Partial transmit sequence based on discrete particle swarm optimization with threshold about PAPR reduction in FBMC/OQAM system. IET Communications. 16(2): 142-150.

[12] Samayoa Yasser and Jörn Ostermann. 2020. Modified active constellation extension algorithm for PAPR reduction in OFDM systems. In 2020 wireless telecommunications symposium (WTS), pp. 1-5. IEEE.

[13] Choi Kwonhue. 2018. Alamouti coding for DFT spreading-based low PAPR FBMC. IEEE Transactions on Wireless Communications. 18(2): 926-941.

[14] Yeh, Hen-Geul and Hannan Mutahir Abdul. 2015. Hadamard SCFDMA-A modified uplink transmission scheme with low PAPR and SER. In 2015 Annual IEEE Systems Conference (SysCon) Proceedings, pp. 711-715. IEEE.

[15] Karthik Kumar Vaigandla and J. Benita. 2022. Novel Algorithm for Nonlinear Distortion Reduction Based on Clipping and Compressive Sensing in OFDM/OQAM System. IJEER. 10(3): 620-626.

[16] Na Dongjun and Kwonhue Choi. 2019. PAPR reduction scheme for FBMC-OQAM without side information. In ICC 2019-2019 IEEE International Conference on Communications (ICC), pp. 1-6. IEEE.

[17] Nissel Ronald and Markus Rupp. 2018. Pruned DFT-spread FBMC: Low PAPR, low latency, high spectral efficiency. IEEE Transactions on Communications. 66(10): 4811-4825.

[18] Hossain Md Najmul, Yosuke Sugiura, Tetsuya Shimamura and Heung-Gyoon Ryu. 2020. DFT-spread OTFS communication system with the reductions of PAPR and nonlinear degradation. Wireless Personal Communications. 115(3): 2211-2228.

[19] Sarkar Mrinmoy, Asok Kumar and Bansibadan Maji. 2021. PAPR reduction using twin symbol hybrid optimization-based PTS and multi-chaotic-DFT sequence-based encryption in CP-OFDM system. Photonic Network Communications. 41: 148-162.

[20] Cho L., Liao H.-.-C and Hsu C.-.-Y. 2018. Adjustable PAPR reduction for DFT-s-OFDM via improved general precoding scheme. Electron. Lett. 54: 903-905. https://doi.org/10.1049/el.2018.0743

[21] Hossain, Md Najmul, Tetsuya Shimamura, Dayoung Kim and Heung-Gyoon Ryu. 2018. Waveform design of DFT-Spread WR-OFDM system for the OOB and PAPR reduction. In 2018 international conference on information and communication Technology convergence (ICTC), pp. 792-796. IEEE.

[22] Tang, Bo, Kaiyu Qin, and Haibo Mei. 2022. A hybrid approach to reduce the PAPR of OFDM signals using clipping and companding. IEEE Access. 8: 18984-18994.

[23] Shekh Faraj, Bana Hassan and Abdulrahman Ikram Siddiq. 2022. A Review of Peak to Average Power

Ratio Reduction Schemes in OFDM Systems. Kirkuk University Journal-Scientific Studies. 17(1): 7-15.

[24] Abdulridha, Sajjad Razzaq and Fadhil S. Hasan. 2022. Hybrid clipping and companding techniques based peak to average power ratio reduction in orthogonal frequency division multiplexing based differential chaos shift keying system. International Journal of Electrical and Computer Engineering (IJECE). 12(3): 2220-2227.

[25] Odukwe P. C., C. B. Mbachu, B. O. Ekengwu and D. K. Onebunne. 2022. Minimizing PAPR of OFDM Signal Using Discrete Cosine Transform and Log Companding. International Journal of Advanced Networking and Applications. 14(2): 5361-5366.

[26] LiuKaiming, Xiaoyan Cui, Zhitong Xing and Yuan'an Liu. 2022. Generalized continuous piecewise linear companding transform design for PAPR reduction in OFDM systems. IEEE Transactions on Broadcasting. 68(3): 780-796.

[27] Xing Zhitong, Yun Li, Aditya S. Rajasekaran, Deyi Peng and Halim Yanikomeroglu. 2022. Variation Approach-Based Nonlinear Companding Scheme for PAPR Reduction in OFDM Systems. IEEE Transactions on Broadcasting. 68(4): 916-926.

[28] Yadav, Ajay Kumar, and Yogendra K. Prajapati. 2022. A Novel Hybrid Technique for PAPR Reduction of Rayleigh Fading Channel Based OFDM System. Wireless Personal Communications. 1-20.

[29] Niwareeba Roland, Mitchell A. Cox and Ling Cheng. 2022. Low complexity hybrid SLM for PAPR mitigation for ACO OFDM. ICT Express. 8(1): 72-76.

[30] Vaigandla Karthik Kumar and Benita J. 2023. Selective Mapping Scheme Based on Modified Forest Optimization Algorithm for PAPR Reduction in FBMC System. Journal of Intelligent & Fuzzy Systems, pp. 1-15, DOI: 10.3233/JIFS-222090.

[31] Akurati Malleswari, Satish Kumar Pentamsetty, and Satya Prasad Kodati. 2022. Optimizing the Reduction of PAPR of OFDM System Using Hybrid Methods. Wireless Personal Communications. 125(3): 2685-2703.

[32] Ramadevi D. and P. Trinatha Rao. 2022. Maximal-Minimum hybrid approach with decomposed SLM technique for 5G UFMC system PAPR reduction. Optik. 270: 169955.

[33] Raveen Panchireddi, and Uppalapati Venkata Ratna Kumari. 2022. A hybrid deep learning using reptile dragonfly search algorithm for reducing the PAPR in OFDM systems. Journal of Optical Communications.

[34] Vaigandla K. K. and Benita J. 2023. A Novel PAPR Reduction in Filter Bank Multi-Carrier (FBMC) with Offset Quadrature Amplitude Modulation (OQAM) Based VLC Systems. International Journal on Recent and Innovation Trends in Computing and Communication, 11(5):288-299. https://doi.org/10.17762/ijritcc.v11i5.6616